Development of 2D Bi-SQUID Arrays with High Linearity

S. Berggren, *Member, IEEE,* G. Prokopenko, P. Longhini, *Member, IEEE,* A. Palacios, O. A. Mukhanov, *Fellow, IEEE,* A. Leese de Escobar, *Member, IEEE,* B. J. Taylor, M. C. de Andrade, *Member, IEEE,* M. Nisenoff, *Life Fellow, IEEE,* R. L. Fagaly, *Fellow, IEEE,* T. Wong, E. Cho, E. Wong, V. In

***Abstract*—We develop a two-dimensional (2D) Superconducting Quantum Interference Filter (SQIF) array based on recently introduced high-linearity tri-junction bi-SQUIDs. Our bi-SQUID SQIF array design is based on a tight integration of individual bi-SQUID cells sharing inductances with adjacent cells. We provide extensive computer simulations, analysis and experimental measurements, in which we explore the phase dynamics and linearity of the array voltage response. The non-uniformity in inductances of the bi-SQUIDs produces a pronounced zero-field single anti-peak in the voltage response. The anti-peak linearity and size can be optimized by varying the critical current of the additional junction of each bi-SQUID. The layout implementation of the tight 2D array integration leads to a distinct geometrical diamond shape formed by the merged dual bi-SQUID cells. Different size 2D arrays are fabricated using standard HYPRES niobium 4.5 kA/cm^2 fabrication process. The measured linearity, power gain, and noise properties will be analyzed for different array sizes and the results will be compared with circuit simulations. We will discuss a design approach for the electrically small magnetic field antenna and low-noise amplifiers with high bandwidth based on these 2D bi-SQUID SQIF arrays. The results from this work will be used to design chips densely and completely covered in bi-SQUIDs that has optimized parameters such as linearity and power gain.**

***Index Terms*—SQUID, numerical simulations, small antenna, low noise amplifier, flux noise, high sensitivity**

I. Introduction

THE quest to increase the linearity of SQUID and SQIF arrays was boosted by the introduction of the bi-SQUID – a tri-junction dc SQUID with a linear voltage response [1]–[3]. A non-linear inductance of the additional third junction provided the desired linearizing effect. These bi-SQUIDs are now being used in uniform and non-uniform (SQIF) arrays in place of conventional dc SQUIDs with a goal of achieving higher linearity. To date, the most of the design efforts using both SQUIDs and bi-SQUIDs went into the optimization of one-dimensional (1D) serial or parallel arrays and their combinations. This is due to the higher complexity analysis and modeling required for 2D arrays to account mutual coupling of neighboring cells and complex current distribution in arrays.

Arrays of DC bi-SQUIDs with size varying from loop to loop in an unconventional geometric structure are known to exhibit a magnetic flux dependent average voltage response $< V(\Phi_e/\Phi_0) >$, where Φ_e denotes the external magnetic flux and Φ_0 is the magnetic flux quantum, that has a pronounced single peak with a large voltage swing at zero magnetic flux. The potential high dynamic range and linearity of the "anti-peak" voltage response render the array a promising candidate for multiple applications including a detector of absolute strength of external magnetic fields, wide-band low noise amplifiers and magnetic antennas. These arrays are also commonly known as Superconducting Quantum Interference Filters (SQIFs). Since it was theoretically proposed [4], [5] and experimentally demonstrated for the first time [6]–[8] the SQIF concept is investigated and exploited by a continuously growing number of groups with respect to its basic properties [9]–[14] and its suitability in various fields of application like magnetometry [15]–[20], low noise amplifiers of radio frequency (RF) and digital signals [21]–[29] and electrically small antennas [30], [31]. The unique noise properties, wide bandwidth and linearity of certain configurations of the SQIF array makes it especially attractive for an integration with superconducting wideband Digital-RF receivers being introduced for a variety of military and civilian applications [32]–[37]. These receivers are based on highly linear superconducting analog-to-digital converters [38]–[40] which require equally high linearity of analog RF electronics.

In this paper, we present a new design for the 2D array – a tightly coupled 2D network of bi-SQUID cells, in which junctions and inductances are shared between adjacent cells. In order to achieve this, we alter the shape (or inductance selection) of the bi-SQUID cells and merge two cells together to form a dual bi-SQUID – a diamond-shaped bi-SQUID. A diamond shape layout of these cells makes 2D array integration easier and allows for the bi-SQUIDs to be more densely packed. We demonstrate numerically and experimentally that these 2D bi-SQUID SQIF arrays can be optimized to produce a linear anti-peak at the zero magnetic flux. We examine in great detail the voltage response as a function of

Manuscript received October 9, 2012. This work is supported in part by the Tactical SIGINT Technology Program N66001-08-D-0154, SPAWAR SBIR contracts N00039-08-C-0024, N66001-09-R-0073, ONR (Code 30), the SPAWAR internal research funding (S&T) program and HYPRES IR&D Program.

S. Berggren and A. Palacios are with San Diego State University, San Diego, CA 92182 USA (e-mail: susan_berggren@yahoo.com).

G. Prokopenko and O. A. Mukhanov are with HYPRES Inc., Elmsford, NY 10523 USA (phone: 914-592-1190; fax: 914-347-2239; e-mail: georgy@hypres.com, mukhanov@hypres.com).

P. Longhini, A. Leese de Escobar, B. J. Taylor, M. C. de Andrade, E. Wong and V. In are with SPAWAR SSC Pacific, San Diego, CA 92152 USA.

M. Nisenoff is with M. Nisenoff Associates, Minneapolis, MN 55403 USA.

R. L. Fagaly is with Quasar Federal Systems, San Diego, CA 92121 USA.

E. Cho and T. Wong are with the University of California, San Diego, La Jolla, CA 92093

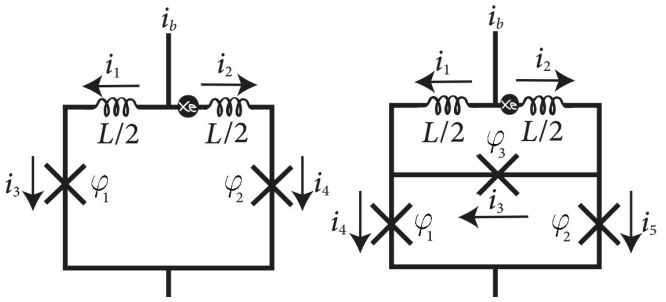

Fig. 1. Schematic diagram of a single DC SQUID (left) and a single DC bi-SQUID (right) where (i_b, i_1, i_2, i_3, i_4, i_5) are the normalized currents, (φ_1, φ_2, φ_3) represent the phases across the Josephson junctions, $L/2$ is the parameter related to the inductance values and x_e is the point in the equations where the external fields are included.

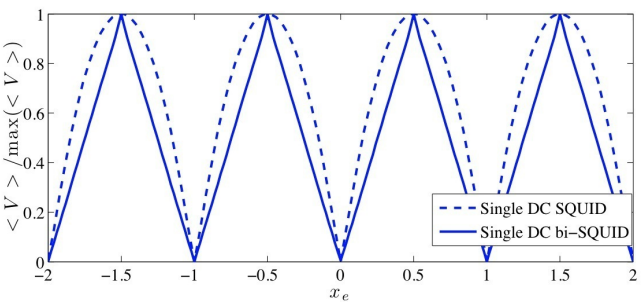

Fig. 2. Average voltage response of a single DC SQUID compared with that of a single DC bi-SQUID. The computer simulations of the system of equations in Eq. (1) and Eq. (2) were performed with $i_b = 2.0$, $L = 1.0$ and $i_{c3} = 1.0$.

controlled parameters, including: inductive coupling between loops, number of loops, bias current, and distribution of loop areas. The results from the numerical analysis are validated against experimental results from fabricated designs.

II. Background: The single SQUID and bi-SQUID

A single DC SQUID has two Josephson junctions arranged in parallel, connected with superconducting material, see the schematic diagram on the left in Fig. 1. The equations are derived using Kirchhoff's current law [41], which is the principle of conservation of electric charge and implies that at any junction in an electrical circuit the sum of currents flowing into that node is equal to the sum of currents flowing out of that node, along with a resistively shunted junction (RSJ) model of the over-damped Josephson junction. The Josephson junctions are assumed to be symmetric, in particular having identical critical currents I_{c1} and i_{c2} that we use to normalize all the other currents in our consideration. The system of equations that models a single SQUID dynamics [42] is

$$\begin{aligned}\dot{\varphi}_1 &= \frac{i_b}{2} - \frac{1}{L}(\varphi_1 - \varphi_2 - \varphi_e) - \sin\varphi_1 \\ \dot{\varphi}_2 &= \frac{i_b}{2} + \frac{1}{L}(\varphi_1 - \varphi_2 - \varphi_e) - \sin\varphi_2, \end{aligned} \tag{1}$$

where φ_1 and φ_2 are the phases across each of the Josephson junctions and the dots denote the time differentiation with normalized time $\tau = \omega_c t$, where t is time and $\omega_c = \frac{2eI_cR_N}{\hbar}$. The parameter R_N in ω_c is the normal state resistance of the Josephson junctions, I_c is the critical current of the Josephson junctions, e is the charge of an electron, and $\hbar$ is the reduced Planck constant. $i_b = \frac{I_b}{I_c}$ is the normalized bias current, where I_b is the bias current. $L = 2\pi\frac{lI_c}{\Phi_0}$ is the normalized inductance and $\varphi_e = 2\pi a x_e$, where $x_e = \frac{B_e}{\Phi_0}$ is the normalized external magnetic flux per unit area and a is the bi-SQUID area. We use the approximate assumption that $a = L$. $\Phi_0 \equiv \frac{h}{2e} \approx 2.07 \times 10^{-15}$ tesla meter squared is the flux quantum, where h is Plank's constant and $2e$ is the charge on the Cooper pair.

A DC bi-SQUID, which is a SQUID with an additional Josephson junction bisecting the superconducting loop, was introduced as an alternative to traditional SQUIDs and have shown superior linearity in the average voltage response anti-peak feature. The phase equations for the single DC bi-SQUID schematic on the right in Fig. 1 are derived in a similar way to those of the single DC SQUID. In this case there is a third junction J_3 that is related to the first and second junctions through the phases: $\varphi_1 + \varphi_3 = \varphi_2$. Using this relationship all the terms that include φ_3 can be replaced with $\varphi_2 - \varphi_1$, thereby reducing the number of phase equations needed to model the system from three to two as shown in [1]. The governing equations for a single bi-SQUID are

$$\begin{aligned}\dot{\varphi}_1 &= \frac{i_b}{2} - \frac{1}{3L}(\varphi_1 - \varphi_2 - \varphi_e) + \frac{1}{3}i_{c3}\sin(\varphi_2 - \varphi_1) \\ &\quad -\frac{2}{3}\sin\varphi_1 - \frac{1}{3}\sin\varphi_2 \\ \dot{\varphi}_2 &= \frac{i_b}{2} + \frac{1}{3L}(\varphi_1 - \varphi_2 - \varphi_e) - \frac{1}{3}i_{c3}\sin(\varphi_2 - \varphi_1) \\ &\quad -\frac{1}{3}\sin\varphi_1 - \frac{2}{3}\sin\varphi_2, \end{aligned} \tag{2}$$

where $i_{c3} = \frac{I_{c3}}{I_c}$, and I_{c3} is the is the critical current of the third junction. All other parameters are defined as the single DC SQUID.

The single DC SQUID and DC bi-SQUID are simulated by integrating the systems of equations that model the system dynamics, Eq. (1) and Eq. (2) respectively. After the phases φ_1 and φ_2 have been determined the derivatives $\dot{\varphi}_1$ and $\dot{\varphi}_2$ are evaluated and the time-dependant voltage $V(t) = \frac{\dot{\varphi}_1 + \dot{\varphi}_2}{2}$ is calculated. The average voltage, $< V >$, of a SQUID (or bi-SQUID) at a point in x_e is the mean value of the voltage over time, presented in Fig. 2. The average voltage response of the bi-SQUID, with the proper selection of parameters, has a more linear average voltage response than the conventional DC SQUIDs. The higher linearity of the average voltage response increases the utility of the device as a linear amplifier.

III. Diamond Shaped bi-SQUID

The repeating pattern in the 2D array is a diamond-shape created by two bi-SQUIDs. Fig. 3 depicts a circuit of a single diamond structure of bi-SQUIDs where (i_b, i_1,...,i_{11}) represent the normalized currents, (φ_1...φ_6) are the phases across the Josephson junctions and (L_1, L_{2a},...,L_{6a}, L_{2b},...,L_{6b}) represent the normalized inductances. To assist with the design of the

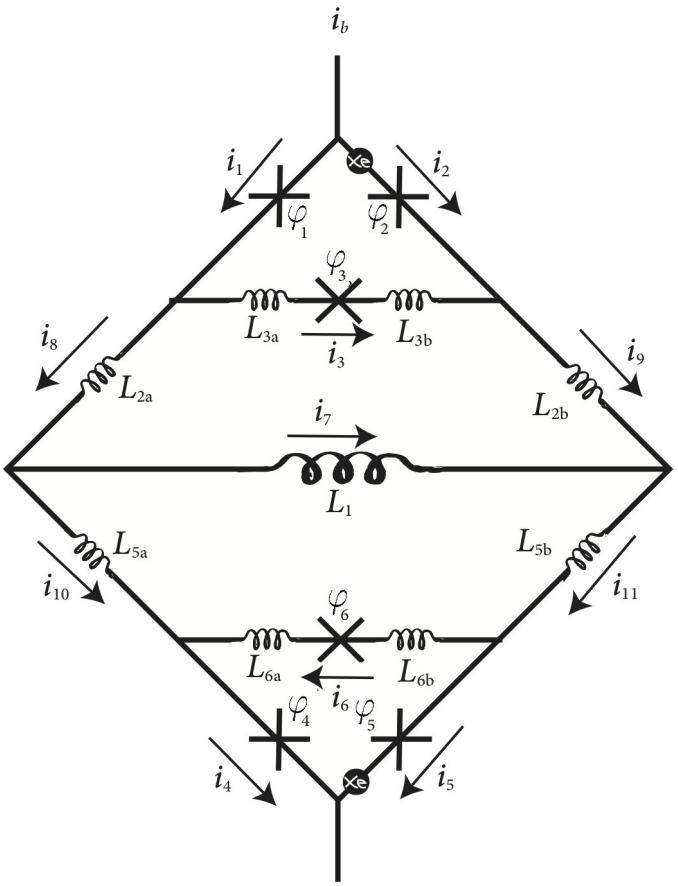

Fig. 3. Single diamond structure of bi-SQUIDs circuit representation where (i_b, i_1,...,i_{11}) are the normalized currents, (φ_1...φ_6) represent the phases across the Josephson junctions, (L_1, L_{2a},...,L_{6a}, L_{2b},...,L_{6b}) are the parameters related to the inductance values and x_e is the point in the equations where the external fields are included.

array, equations that model the system are derived to be used in computer simulations test the effects of different parameter values. Six governing equations are needed to simulate the average voltage response for a single diamond structure of bi-SQUIDs, which contains six Josephson junctions and nine inductors.

Kirchhoff's current law results in the following relations for the currents and phases in the diamond-shaped dual bi-SQUID

$$\begin{aligned}
&i_b = i_1 + i_2 && i_1 = i_3 + i_8 \\
&i_2 + i_3 = i_9 && i_8 = i_7 + i_{10} \\
&i_9 + i_7 = i_{11} && i_{10} + i_6 = i_4 \\
&i_{11} = i_6 + i_5 && i_4 + i_5 = i_b \\
&i_1 = \sin\varphi_1 + \dot{\varphi}_1 && i_2 = \sin\varphi_2 + \dot{\varphi}_2 \\
&i_4 = \sin\varphi_4 + \dot{\varphi}_4 && i_5 = \sin\varphi_5 + \dot{\varphi}_5 \\
&i_3 = i_{c3}\sin\varphi_3 + \dot{\varphi}_3 && i_6 = i_{c6}\sin\varphi_6 + \dot{\varphi}_6,
\end{aligned} \tag{3}$$

where φ_i are the phases across of the Josephson junctions, $i = 1, ..., 6$. I_{ci} are the critical currents of each of the junctions, $i = 1, ..., 6$, that satisfy $I_{c1} = I_{c2} = I_{c4} = I_{c5} = I_c$. $i_{c3} = I_{c3}/I_c$ is the normalized critical current of the third junction and $i_{c6} = I_{c6}/I_c$ is the normalized critical current of the sixth junction. The dot denotes time differentiation with normalized time $\tau = \omega_c t$. Applying the mesh rule for the phase of the macroscopic wave function of the Cooper pairs to the top half of the diamond gives

$$\varphi_1 + L_1 i_7 + L_{2a} i_8 = 2\pi x_e a_1 + \varphi_2 + L_{2b} i_9,$$

where $\varphi_e = 2\pi a_1 x_e$, where x_e is the normalized external magnetic flux and we use the approximate assumption that $a_1 = L_1 + L_{2a} + L_{2b}$. Combining $i_7 = i_8 - i_{10}$ and $i_7 = i_{11} - i_9$ such that $i_7 = \frac{i_8 - i_{10}}{2} + \frac{i_{11} - i_9}{2}$, and then substituting the current relations for i_7, i_{10}, i_9, and i_8 yields

$$\begin{aligned}
&\left(\frac{L_1}{2} + L_{2a}\right) i_1 - \frac{L_1}{2} i_4 + \frac{L_1}{2} i_5 + L_1 i_6 = \varphi_2 - \varphi_1 \\
&+ \left(\frac{L_1}{2} + L_{2b}\right) i_2 + 2\pi x_e a_1 + (L_1 + L_{2a} + L_{2b})\, i_3.
\end{aligned} \tag{4}$$

In order to get the first of the six equations that is needed to describe the dynamics of the diamond shape, the bias current relation $i_2 = i_b - i_1$ and Josephson junction relations from Eq. (3) are substituted into Eq. (4) to become

$$\begin{aligned}
L_{12}(\dot{\varphi}_1 - \dot{\varphi}_3) + \frac{L_1}{2}(2\dot{\varphi}_6 + \dot{\varphi}_5 - \dot{\varphi}_4) &= \left(\frac{L_1}{2} + L_{2b}\right) i_b \\
&+ \varphi_2 - \varphi_1 + 2\pi x_e a_1 + L_{12}\left(i_{c3}\sin\varphi_3 - \sin\varphi_1\right) \\
&+ \frac{L_1}{2}\left(\sin\varphi_4 - \sin\varphi_5 - 2i_{c6}\sin\varphi_6\right),
\end{aligned} \tag{5}$$

where $L_{12} = L_1 + L_{2a} + L_{2b}$. To solve for the second of the six equations that governs the dynamics of the single diamond the current relations for the bias current $i_1 = i_b - i_2$ and Josephson junctions from Eq. (3) are substituted into Eq. (4) to give

$$\begin{aligned}
\frac{L_1}{2}(2\dot{\varphi}_6 + \dot{\varphi}_5 - \dot{\varphi}_4) - L_{12}(\dot{\varphi}_2 + \dot{\varphi}_3) &= -\left(\frac{L_1}{2} + L_{2a}\right) i_b \\
&+ \varphi_2 - \varphi_1 + 2\pi x_e a_1 + L_{12}\left(i_{c3}\sin\varphi_3 + \sin\varphi_2\right) \\
&+ \frac{L_1}{2}\left(\sin\varphi_4 - \sin\varphi_5 - 2i_{c6}\sin\varphi_6\right).
\end{aligned} \tag{6}$$

The current-phase relation around the upper loop in the single diamond is

$$\varphi_1 + \varphi_3 + L_3 i_3 = \varphi_2,$$

where $L_3 = L_{3a} + L_{3b}$. Substituting the Josephson junction relations from Eq. (3) and reorganizing yields the third of the six equations for the dynamics of the single diamond.

$$L_3\dot{\varphi}_3 = \varphi_2 - \varphi_1 - \varphi_3 - L_3 i_{c3}\sin\varphi_3. \tag{7}$$

A similar procedure is used to determine the equations for the three junctions located in the bottom half of the diamond structure and can be combined with the equations from Eqs. (5) - (7) to obtain the full system of equations that governs the phase dynamics of the diamond-shaped bi-SQUID

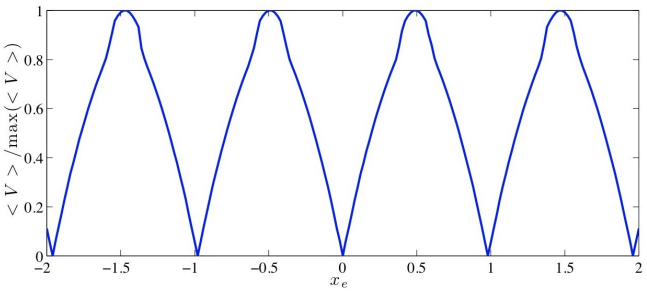

Fig. 4. Calculated average voltage response of a single diamond shaped DC SQUID, performed with $i_b = 2.0$, $L_1 = 0.54$, $L_{2a} = L_{2b} = L_{5a} = L_{5b} = 0.24$, $L_{3a} = L_{3b} = L_{6a} = L_{6b} = 0.3$ and $i_{c3} = 0.5$.

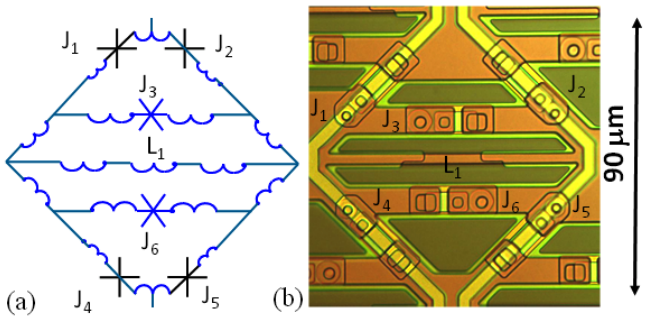

Fig. 5. Diamond-shaped dual bi-SQUID: (a) cell schematic; (b) microphotograph of the fabricated cell within a 2D array. $I_c = 0.25$ mA, $R_{\rm sh} = 2.4$ Ω , $V_c = I_c R_{sh} = 600$ μV. All junctions are critically shunted, $\beta_c = 1$.

$$
\begin{aligned}
&L_{12}(\dot\varphi_1 - \dot\varphi_3) + \frac{L_1}{2}(2\dot\varphi_6 + \dot\varphi_5 - \dot\varphi_4) = \left(\frac{L_1}{2} + L_{2b}\right) i_b \\
&\quad + \varphi_2 - \varphi_1 + 2\pi x_e a_1 + L_{12}\left(i_{c3}\sin\varphi_3 - \sin\varphi_1\right) \\
&\quad + \frac{L_1}{2}\left(\sin\varphi_4 - \sin\varphi_5 - 2i_{c6}\sin\varphi_6\right) \\
&\frac{L_1}{2}(2\dot\varphi_6 + \dot\varphi_5 - \dot\varphi_4) - L_{12}(\dot\varphi_2 + \dot\varphi_3) = -\left(\frac{L_1}{2} + L_{2a}\right) i_b \\
&\quad + \varphi_2 - \varphi_1 + 2\pi x_e a_1 + L_{12}\left(i_{c3}\sin\varphi_3 + \sin\varphi_2\right) \\
&\quad + \frac{L_1}{2}\left(\sin\varphi_4 - \sin\varphi_5 - 2i_{c6}\sin\varphi_6\right) \\
&L_3\dot\varphi_3 = \varphi_2 - \varphi_1 - \varphi_3 - L_3 i_{c3}\sin\varphi_3 \\
&L_{15}(\dot\varphi_4 - \dot\varphi_6) + \frac{L_1}{2}(2\dot\varphi_3 + \dot\varphi_2 - \dot\varphi_1) = \left(L_{5b} + \frac{L_1}{2}\right) i_b \\
&\quad + \varphi_5 - \varphi_4 + 2\pi x_e a_2 + L_{15}\left(i_{c6}\sin\varphi_6 - \sin\varphi_4\right) \\
&\quad + \frac{L_1}{2}\left(\sin\varphi_1 - \sin\varphi_2 - 2i_{c3}\sin\varphi_3\right) \\
&\frac{L_1}{2}(2\dot\varphi_3 + \dot\varphi_2 - \dot\varphi_1) - L_{15}(\dot\varphi_5 + \dot\varphi_6) = -\left(L_{5b} + \frac{L_1}{2}\right) i_b \\
&\quad + \varphi_5 - \varphi_4 + 2\pi x_e a_2 + L_{15}\left(i_{c6}\sin\varphi_6 + \sin\varphi_5\right) \\
&\quad + \frac{L_1}{2}\left(\sin\varphi_1 - \sin\varphi_2 - 2i_{c3}\sin\varphi_3\right) \\
&L_6\dot\varphi_6 = \varphi_5 - \varphi_4 - \varphi_6 - L_6 i_{c3}\sin\varphi_3, \qquad (8)
\end{aligned}
$$

where $L_{15} = L_1 + L_{5a} + L_{5b}$, $L_6 = L_{6a} + L_{6b}$ and we use the approximate assumption that $a_2 = L_1 + L_{5a} + L_{5b}$.

The calculated average voltage response for the diamond shape is shown in Fig. 4. This average voltage response is more linear than the single SQUID but less so than the single bi-SQUID, shown in Fig. 2. The non-linearities are most likely due to the inclusion of additional inductances in the diamond structure of bi-SQUIDs. The analysis is now extended to the full 2D diamond array. The phase equations that model the 2D diamond arrays are derived in a similar way as the single diamond structure of bi-SQUIDs. These modeling equations total 66. Both the system of equations and the derivations are not expressed explicitly for brevity.

IV. Implementation of 2D Diamond bi-SQUID Arrays

For experimental evaluation of our 2D SQIF arrays of diamond-shaped dual bi-SQUID cells, various size arrays were laid out. Fig. 5 shows a schematic and a layout of the diamond-shaped dual bi-SQUID cell designed for a standard HYPRES Nb fabrication process [43]–[45]. $R_{\rm sh}$ is the shunting resistance and V_c is the critical voltage across each of the junctions. Its electrical circuit was extracted and re-simulated to account for the actual layout parameters. The layout was done using all four available Nb layers: a ground plane layer, two layers for junctions and inductors, and a top layer to implement a flux bias line overlaying bi-SQUID cells (two light gray strips retracing the diamond cell contour). The ground plane was used only under Nb layers forming bi-SQUID inductors and junctions in order to maintain their low specific inductance. However, ground plane was partially removed from under inductor L_1 to increase its value if desired. The ground plane was also removed from the central area of the bi-SQUID loops to allow an external magnetic field to thread through the cell (dark areas in Fig. 5(b)). The total area of the dual-bi-SQUID cell is $\sim$ 1623 μm^2. While the total area of the cell is kept the same, the values of inductances are varied by their width and ground plane opening size under L_1. We designed arrays with normal Gaussian distribution of cell inductances with σ $\sim$ 30% and $\sim$ 70% for comparison.

Fig. 6 shows a schematic and the layout implementation for a 2D array using diamond dual bi-SQUID cells. It is evident that a diamond shape of our dual bi-SQUID cells leads to their natural 2D arrangement into a diamond checkered pattern by connecting dual bi-SQUID cells by their corners. The space between cells forms a similar array comprising dual bi-SQUIDs with somewhat different ratio of inductors forming bi-SQUID loops. As a result, each bi-SQUID shares its junctions (J_1 and J_2) and inductances with neighboring bi-SQUIDs. Each dual bi-SQUID has a contact to three neighboring cells at each of four corners (8 in total). This 2D array design avoids the use of long parasitic wires, as every component of the array is an essential element of a bi-SQUID indicating to an efficient use of the available area.

The array dc bias is fed uniformly from the top bi-SQUID row of the array. Similarly, the array is grounded to the bottom bi-SQUID row. The inductively coupled flux bias line is overlayed on the top of the array forming loops for each column. The direction of the dc flux bias control current is shown by small arrows in Fig. 6(b). This line can be used for RF signal input for testing in the low noise amplifier regime,

while the output signal is measured at the dc bias current terminal via a bias tee.

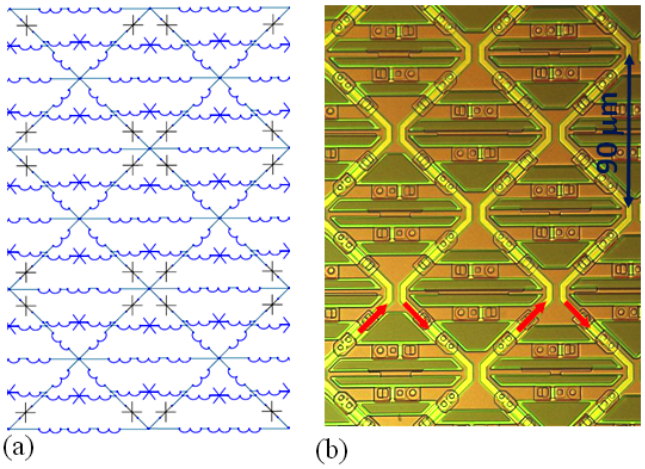

Fig. 6. 2D diamond-shaped bi-SQUID array: (a) 2D array schematic; (b) microphotograph of the fabricated 2D array.

Fig. 7 shows microphotographs of some examples of the fabricated 2D bi-SQUID SQIF arrays with different size and configuration. We chose to resistively shunt all junctions in the bi-SQUIDs in the arrays shown. The objective of these designs is to investigate the array dimension dependences. Only 12 contact pads are used. These are concentrated on one side of the chip in preparation for antenna tests in which RF signal will be irradiated to the chip. To investigate the array characteristics, several test arrays with different sizes and configurations were laid out using 5×5 mm^2 chips for the fabrication with a 4.5 kA/cm^2 Josephson junction critical current density.

V. Experimental Evaluation as a Low Noise Amplifier

Experimental evaluation was first performed in liquid helium using the test setup described in detail in [46]. Each chip was tested using HYPRES standard cryoprobes with 40 coaxial lines. These cryoprobes can make contact only to the required smaller number (12) of pads (Fig. 7) without shorting the array structure by remaining 38 unused cryoprobe contacts.

A. Experimental Investigation of Noise Properties

Fig. 8(a) shows the measured flux-to-voltage characteristics of the 15×80 bi-SQUID array with a 70% inductance spread shown in Fig. 7(a). As one can see, it has a well-defined zero-field anti-peak. Fig. 8(b) shows the corresponding flux noise measurement at the mid-point of the positive slope of the anti-peak. The flux noise spectral density is reaching to $\sim 2 \times 10^{-6}\Phi_0/\sqrt{\text{Hz}}$, which is the expected value for this array. Fig. 9 shows the corresponding energy sensitivity and noise temperature calculated following [47], [48].

The noise energy per unit bandwidth via flux noise in a SQUID is

$$\varepsilon(f) = \frac{S_\Phi(f)}{2L}, \tag{9}$$

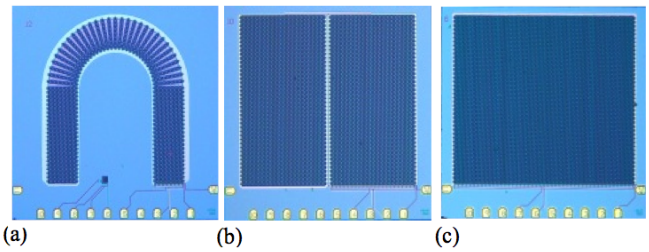

Fig. 7. Microphotographs of 5×5 mm^2 chips of different 2D diamond bi-SQUID SQIF arrays with a $\sigma \sim 70\%$ spread: (a) a 1200 bi-SQUID (15×80) array; (b) two serially connected 2D arrays ($2 \times 43 \times 85$) arrays with 7310 bi-SQUIDs; (c) a single 7820 bi-SQUID (92×85) 2D array. The sizes of these arrays are calculated by assuming each diamond has two bi-SQUIDs.

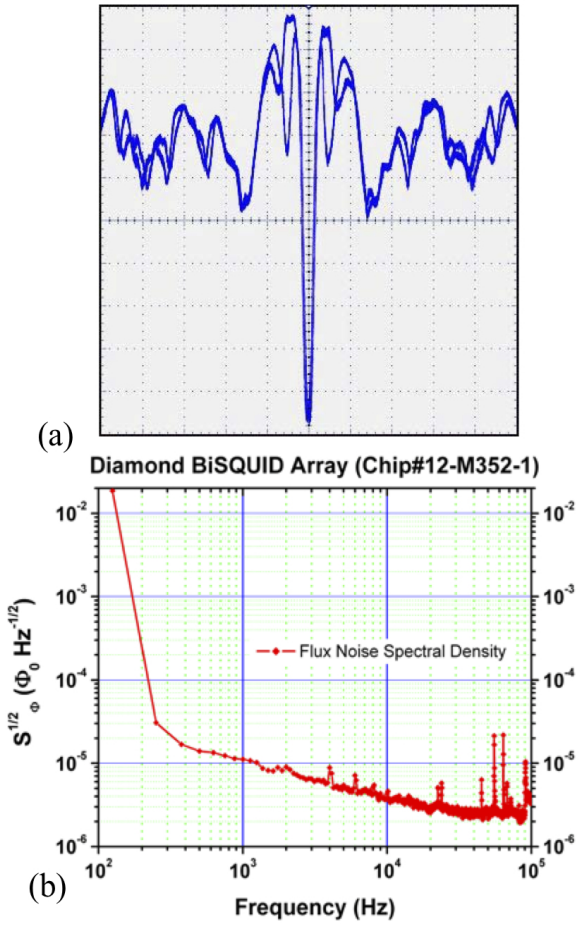

Fig. 8. Measured characteristics of a 15×80 cell dual bi-SQUID SQIF array of Fig. 7(a) with $\sigma \sim 70\%$ of inductance spread: (a) flux/voltage characteristic with 2 mV/div 0.5 mA/div, max voltage $\approx$ 18 mV, ΔV/ΔI (flux bias) $\approx$ 170 V/A. (b) measured flux noise spectral density. The spikes are attributed to a noisy frequency generator.

where f is frequency. The inductance, L, of bi-SQUID is calculated from the measured separately ΔI_c modulations of the IV curve defined as $L = \frac{\Phi_0}{2\Delta I_c}$. The noise temperature can be expressed as

$$T_N = \frac{\pi f \varepsilon(f)}{k_B}, \tag{10}$$

where k_B is Boltzmann's constant. The quantum limit of noise temperature is defined as $T_{QL} = \frac{1}{2}hf/k_B$ [49]. The upper frequency (100 kHz) for our sensitivity measurements was determined by the available test equipment. However, the

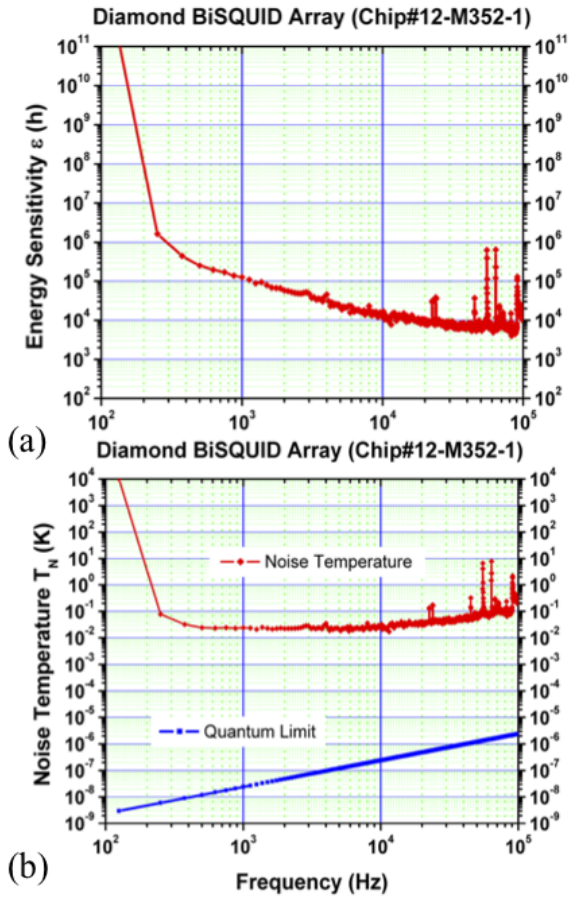

Fig. 9. Noise characteristics of the 1200 (15×80) bi-SQUID SQIF array shown in Fig. 7(a): (a) energy sensitivity; (b) noise temperature compared against quantum limit.

noise temperature has a linear frequency dependence for given device, e. g., for a SQUID RF amplifier, T_N scales as the ratio $\omega_0/V(\Phi)$ [50]. So, one can extrapolate the noise data obtained at lower frequencies (100 kHz) to higher frequencies and estimate the noise properties up to, e.g., ~ 2 GHz, which is still much lower than Josephson frequency at the DC bias point.

B. Experimental Results Compared Against Simulations

For comparison to results of simulation described above, the arrays chips were fabricated with a 30% and 70% Gaussian spread in inductances. Figs. 10 and 11 show that increasing the Gaussian spread to 70% makes the average voltage response go from a wave packet-like response to a single anti-peak. The single anti-peak is the form of the average voltage response in which we are interested. The generation of the single anti-peak feature is significant because the anti-peak was obtained with identical size bi-SQUID loops and with varying the inductances. The fabricated arrays that produced the current flux/voltage characteristic in Figs. 10 and 11 were 15×40 and 15×80 arrays, respectively. While the simulations were performed with arrays of size 3×80. To simulate larger arrays the code will need to be parallelized.

A comparison of the experimental and simulated current flux/voltage characteristic was performed on an array of size

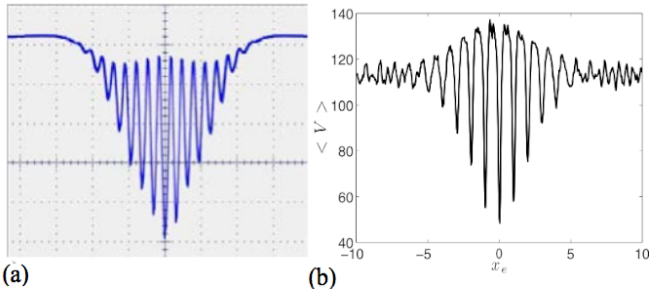

Fig. 10. Comparison of the (a) measured (5 mV/div, 10 mA/div) for a 15×40 dual bi-SQUID array and (b) simulated flux (control current)/voltage characteristic for $\sigma \sim 30\%$. The simulations were performed using a 3×80 array with $i_b = 2.0$ and $i_{c3} = 1.0$.

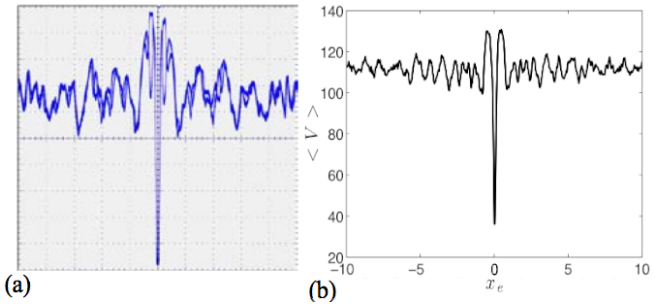

Fig. 11. Comparison of the (a) measured (2 mV/div, 1 mA/div) for a 15×80 dual bi-SQUID array and (b) simulated flux (control current)/voltage characteristic for $\sigma \sim 70\%$. The simulations were performed using a 3×80 array with $i_b = 2.0$ and $i_{c3} = 1.0$.

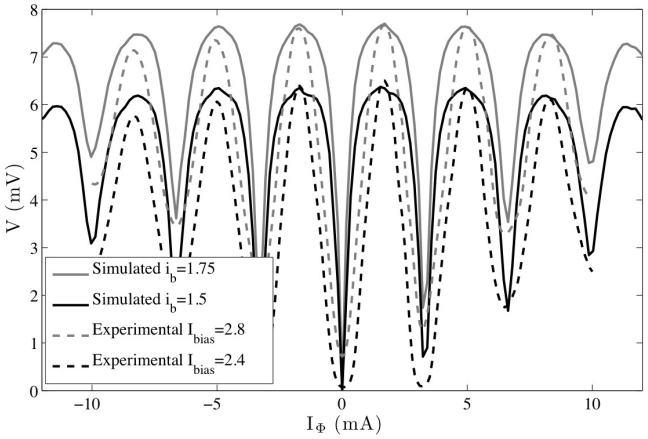

Fig. 12. Comparison of the measured and simulated control current flux/voltage characteristic for a 15×20 diamond array with the inductances spread $\sigma \sim 30\%$. The measurements of the fabricated array were performed with $I_{bias} = 2.4$ and 2.8. The simulations were performed with $i_b = 1.5$ and 1.75 and $i_{c3} = 0.5$.

15×20, see Fig. 12. While there are many similarities, the difference in the width of the peaks is most likely due to the array having unshunted third Josephson junctions while the system of equations that model the system are derived using all resistively shunted junctions.

C. Experimental LNA response

Measurements of the input power and output power for single tone frequencies were performed 5.3 MHz, 208 MHz, and 413 MHz at the CERF Center of Excellence on a 7×80 array with a 30% Gaussian spread in inductances and unshunted

TABLE I
SQIF LNA OUTPUT TO SINGLE RF CW TONES

Input Power 5.3 Mhz (dBm)	Normalized Power Output (dB)
-100	–
-80	25
-60	42.5
Input Power 208 Mhz (dBm)	Normalized Power Output (dB)
-100	0
-80	14
-60	34
Input Power 413 Mhz (dBm)	Normalized Power Output (dB)
-100	–
-80	15
-60	34.5

Table of power input and output values to a single tone at frequencies 5.3 MHz, 208 MHz, and 413 MHz.

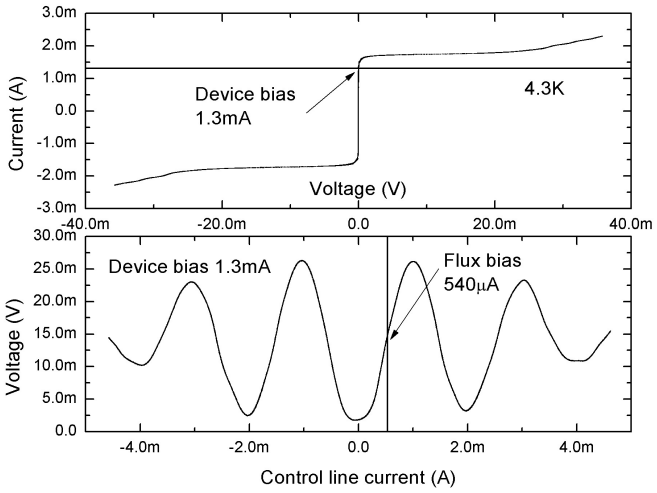

Fig. 13. Visualization of the points of device bias and flux bias for measurements.

third junctions, see Table I. The measurements were performed with the output power normalized to the lowest observable power, which was about -126.4 dBm, corresponding to an input power of -100 dBm at 208 MHz, current bias of 1.3 mA, and flux bias from a control line current of 0.54 mA, see Fig. 13. More measurements will need to be performed to determine how the device is performing as an LNA, however the data will be useful when characterizing devices in the near future (for RF studies).

D. Antenna Sensitivity Analysis

We estimated possible antenna sensitivities for a SQIF-based antenna by assuming that the area for the diamond shaped (double) bi-SQUID is 1.62×10^{-9} m^2. Using that as the effective area, multiplying by $15 \times 80/2$ to account for the number of individual bi-SQUIDs in the array, and taking the flux noise from Fig. 8(b) as 2×10^{-6} $\Phi_0/\sqrt{\text{Hz}}$, gives a field sensitivity of ~ 4.25 fT$/\sqrt{\text{Hz}}$.

Assuming a scaling as $\sqrt{N}$, the field noise for a 1000×2000 array would be 0.104 fT$/\sqrt{\text{Hz}}$ at 100 kHz. Approximating the physical dimension of the diamond as ~ 71 μm $\times$ 71 μm means that the diamond occupies an area of $\sim 5 \times 10^{-9}$ m^2 (consistent with the effective area of the diamond shaped bi-SQUID). Thus a 1000×2000 array would occupy an area of ~ 50 cm^2, since each diamond contains two bi-SQUIDs. This corresponds to a square with 7.1 cm on a side.

VI. CONCLUSION

We have introduced a new design of 2D SQIF arrays using tightly-coupled diamond-shaped dual bi-SQUID cells. This design allowed us to address the challenge of preserving and enhancing the linearity of individual bi-SQUIDs which tends to be degraded when bi-SQUID cells are connected in parallel. Another advantage of this approach is that the cells can be densely packed onto a chip, resulting in many more bi-SQUIDs in the same area when compared with strings of bi-SQUIDs coupled in series. Our SQIF array design involves bi-SQUIDs with identical areas and varying inductances. We were able to show that a anti-peak feature can be generated with these features. This approach may be applicable for arraying conventional SQUIDs as well.

A system of equations was derived to model the dynamics of the 2D diamond dual bi-SQUID array. The model was very complex and to model large arrays the Matlab code will need to be parallelized. We found a good match between simulations of small arrays and experimental results. The array design has undergone extensive computer simulations, analysis and experimental measurements, in which we explored the voltage response of the 2D arrays.

Experimental measurements were performed on the noise properties of the array design. The results matched the expected values. More extensive experimentation with larger size arrays of different configurations are required in order to optimize the array design to meet the requirements of wide band low noise amplifiers and electrically small antennas. Ongoing work includes Transverse ElectroMagnetic (TEM) cell measurements to experimentally evaluate the array design as an antenna.

ACKNOWLEDGMENT

The authors are grateful to D. Bowling, J. Talvacchio, J. Przybysz for useful discussions, S. Cybart, A. Matlashov, M. Mueck for advice in testing, and HYPRES fabrication team of D. Yohannes, J. Vivalda, R. Hunt, and D. Donnelly for manufacturing the integrated circuits.

REFERENCES

[1] V. K. Kornev, I. I. Soloviev, N. V. Klenov, and O. A. Mukhanov, "Bi-SQUID: a novel linearization method for dc SQUID voltage response," *Superconductor Science and Technology*, vol. 22, pp. 114 011 1–6, Oct. 2009.

[2] V. K. Kornev, I. I. Soloviev, N. V. Klenov, and O. A. Mukhanov, "Progress in high-linearity multi-element josephson structures," *Physica C*, vol. 19, pp. 886–889, Oct. 2010.

[3] I. I. Soloviev, V. K. Kornev, N. V. Klenov, and O. A. Mukhanov, "Superconducting josephson structures with high linearity of transformation of magnetic signal into voltage," *Physics of the Solid State*, vol. 11, pp. 2252–2258, 2010.

[4] J. Oppenländer, C. Häussler, and N. Schopohl, "Non-ϕ_0-periodic macroscopic quantum interference in one-dimensional parallel josephson junction arrays with unconventional grating structure," *Physical Review B*, vol. 63, pp. 024 511 1–9, 2000.

[5] C. Häussler, J. Oppenländer, and N. Schopohl, "Nonperiodic flux to voltage conversion of series arrays of DC superconducting quantum interference devices," *J. Appl. Phys.*, vol. 89, no. 3, pp. 1875–1879, 2001.

[6] T. Träuble, J. Oppenländer, C. Häussler, and N. Schopohl, "Highly sensitive magnetometers for absolute magnetic field measurements based on quantum interference filters," *Physica C*, vol. 368, pp. 119–124, 2002.

[7] J. Oppenländer, C. Häussler, T. Träuble, P. Caputo, J. Tomes, A. Friesch, and N. Schopohl, "Two dimensional superconducting quantum interference filters," *IEEE Trans. Appl. Supercond.*, vol. 13, no. 2, pp. 771 – 774, Jun. 2003.

[8] J. Oppenländer, T. Träuble, C. Häussler, and N. Schopohl, "Superconducting multiple loop quantum interferometers," *IEEE Trans. Appl. Supercond.*, vol. 11, pp. 1271–1274, 2001.

[9] J. Oppenländer, C. Häussler, A. Friesch, J. Tomes, P. Caputo, T. Träuble, and N. Schopohl, "Superconducting quantum interference filters operated in commercial miniature cryocoolers," *IEEE Trans. Appl. Supercond.*, vol. 15, no. 2, pp. 936–939, Jun. 2005.

[10] V. K. Kornev, I. I. Soloviev, J. Oppenländer, C. Häussler, and N. Schopohl, "The oscillation linewidth and noise characteristics of a parallel superconducting quantum interference filter," *Superconductor Science and Technology*, vol. 17, no. 5, pp. S406–S409, 2004.

[11] V. K. Kornev, I. I. Soloviev, N. V. Klenov, and O. A. Mukhanov, "High linearity SQIF-like josephson-junction structures," *IEEE Trans. on Appl. Supercond*, vol. 19, no. 3, pp. 741 –744, Jun. 2009.

[12] V. K. Kornev, I. I. Soloviev, N. V. Klenov, and O. A. Mukhanov, "Synthesis of high-linearity array structures," *Supercond. Sci. and Technol.*, vol. 20, pp. S362–S366, Nov. 2007.

[13] V. K. Kornev, I. I. Soloviev, N. V. Klenov, and O. A. Mukhanov, "High linearity josephson-junction array structures," *Physica C*, vol. 468, pp. 813–816, Apr. 2008.

[14] V. K. Kornev, I. I. Soloviev, N. V. Klenov, and O. A. Mukhanov, "Design and experimental evaluation of SQIF arrays with linear voltage response," *IEEE Trans. Appl. Supercond.*, vol. 21, no. 3, pp. 394–398, Jun. 2011.

[15] V. Schultze, R. IJsselsteijn, H.-G. Meyer, J. Oppenländer, C. Häussler, and N. Schopohl, "High-T_c superconducting quantum interference filters for sensitive magnetometers," *IEEE Trans. Appl. Supercond.*, vol. 13, no. 2, pp. 775 – 778, Jun. 2003.

[16] V. Schultze, R. IJsselsteijn, and H. G. Meyer, "How to puzzle out a good high-t_c superconducting quantum interference filter," *Superconductor Science and Technology*, vol. 19, pp. S411–S415, 2006.

[17] J. Oppenländer, P. Caputo, C. Häussler, T. Träuble, J. Tomes, A. Friesch, and N. Schopohl, "Effects of magnetic field on two-dimensional superconducting quantum interference filters," *Appl. Phys. Lett.*, vol. 83, pp. 969–971, 2003.

[18] P. Caputo, J. Oppenländer, C. Häussler, J. Tomes, A. Friesch, T. Träuble, and N. Schopohl, "High performance magnetic field sensor based on superconducting quantum interference filters," *Appl. Phys. Lett.*, vol. 85, pp. 1389–1391, 2004.

[19] P. Caputo, J. Tomes, J. Oppenländer, C. Häussler, A. Friesch, T. Träuble, and N. Schopohl, "Superconducting quantum interference filters as absolute magnetic field sensors," *IEEE Trans. Appl. Supercond.*, vol. 15, no. 2, pp. 1044–1047, 2005.

[20] Y. Polyakov, V. Semenov, and S. Tolpygo, "3d active demagnetization of cold magnetic shields," *IEEE Trans. Appl. Supercond.*, vol. 21, no. 3, pp. 724–727, 2011.

[21] P. Caputo, J. Tomes, J. Oppenländer, C. Häussler, A. Friesch, T. Träuble, and N. Schopohl, "Two tone response in superconducting quantum interference filters," *IEEE Trans. Appl. Supercond.*, vol. 17, pp. 722–725, 2007.

[22] V. K. Kornev, I. I. Soloviev, N. V. Klenov, T. Filippov, H. Engseth, and O. A. Mukhanov, "Performance advantages and design issues of SQIFs for microwave applications," *IEEE Trans. Appl. Supercond.*, vol. 19, no. 3, pp. 916 –919, Jun. 2009.

[23] P. Caputo, J. Tomes, J. Oppenländer, C. Häussler, A. Friesch, T. Träuble, and N. Schopohl, "Quadratic mixing of radio frequency signals using superconducting quantum interference filter," *Appl. Phys. Lett.*, vol. 89, pp. 062 507 1–3, 2006.

[24] P. Caputo, J. Tomes, J. Oppenländer, C. Häussler, A. Friesch, T. Träuble, and N. Schopohl, "Two-tone response of radiofrequency signals using the voltage output of a superconducting quantum interference filter," *Journal of Superconductivity and Novel Magnetism*, vol. 20, no. 1, pp. 25–30, 2007.

[25] A. Shadrin, K. Constantinian, and G. Ovsyannikov, "Quantum interference filters based on oxide superconductor junctions for microwave applications," *Technical Physics Letters*, vol. 33, no. 3, pp. 192–195, 2007.

[26] A. K. Kalabukhov, M. L. Chukharkin, A. A. Deleniv, D. Winkler, I. A. Volkov, and O. V. Snigirev, "Analysis of the possibility to amplify an RF signal with a superconducting quantum interference filter," *Journal of Communications Technology and Electronics*, vol. 53, no. 8, pp. 934–940, 2008.

[27] V. K. Kornev, I. I. Soloviev, and O. A. Mukhanov, "Possible approach to the driver design based on series SQIF," *IEEE Trans. Appl. Supercond.*, vol. 15, pp. 388–391, Jun. 2005.

[28] V. K. Kornev, I. I. Soloviev, N. V. Klenov, and O. A. Mukhanov, "Development of SQIF-based output broad band amplifier," *IEEE Trans. Appl. Supercond.*, vol. 17, pp. 569–572, Jun. 2007.

[29] O. V. Snigirev, M. L. Chukharkin, A. S. Kalabukhov, M. A. Tarasov, A. A. Deleniv, O. A. Mukhanov, and D. Winkler, "Superconducting quantum interference filters as RF amplifiers," *IEEE Trans. Appl. Supercond.*, vol. 17, pp. 718–721, Jun. 2007.

[30] V. K. Kornev, I. I. Soloviev, N. V. Klenov, A. V. Sharafiev, and O. A. Mukhanov, "Linear bi-SQUID arrays for electrically small antennas," *IEEE Trans. Appl. Supercond.*, vol. 21, no. 3, Jun. 2011.

[31] V. K. Kornev, I. I. Soloviev, N. V. Klenov, A. V. Sharafiev, and O. A. Mukhanov, "Array designs for active electrically small superconductive antennas," *Physica C: Superconductivity*, vol. 479, pp. 119–122, Jan. 2012.

[32] D. K. Brock, O. A. Mukhanov, and J. Rosa, "Superconductor digital RF development for software radio," *IEEE Communications Mag.*, vol. 39, pp. 174–179, Feb. 2001.

[33] D. Gupta, T. V. Filippov, A. F. Kirichenko, D. E. Kirichenko, I. V. Vernik, A. Sahu, S. Sarwana, P. Shevchenko, A. Talalaevskii, and O. A. Mukhanov, "Digital channelizing radio frequency receiver," *IEEE Trans. Appl. Supercond.*, vol. 17, pp. 430–437, Jun. 2007.

[34] O. A. Mukhanov, D. Kirichenko, I. V. Vernik, T. V. Filippov, A. Kirichenko, R. Webber, V. Dotsenko, A. Talalaevskii, J. C. Tang, A. Sahu, P. Shevchenko, R. Miller, S. B. Kaplan, S. Sarwana, and D. Gupta, "Superconductor digital-rf receiver systems," *IEICE Trans. Electron.*, vol. E91-C, pp. 306–317, Mar. 2008.

[35] A. L. de Escobar, R. Hitt, O. A. Mukhanov, and W. Littlefield, "High performance HF-UHF all digital RF receiver tested at 20 ghz clock frequencies," Oct. 2006, in: *Military Comm. Conf. (MILCOM06)*, Washington, DC, USA.

[36] J. Wong, R. Dunnegan, D. Gupta, D. Kirichenko, V. Dotsenko, R. Webber, R. Miller, O. A. Mukhanov, and R. Hitt, "High performance, all digital RF receiver tested at 7.5 gigahertz," Oct. 2007, in: *Military Comm. Conf. (MILCOM07)*, Orlando, FL, USA.

[37] V. Vernik, D. E. Kirichenko, V. V. Dotsenko, R. Miller, R. J. Webber, P. Shevchenko, A. Talalaevskii, D. Gupta, and O. A. Mukhanov, "Cryocooled wideband digital channelizing RF receiver based on low-pass ADC," *Supercond. Sci. and Technol.*, vol. 20, pp. S323–S327, Nov. 2007.

[38] O. Mukhanov, D. Gupta, A. Kadin, and V. Semenov, "Superconductor analog-to-digital converters," *Proc. of the IEEE.*, vol. 92, pp. 1564–1584, Oct. 2004.

[39] A. Inamdar, S. Rylov, A. Talalaevskii, A. Sahu, S. Sarwana, D. E. Kirichenko, I. V. Vernik, T. V. Filippov, and D. Gupta, "Progress in design of improved high dynamic range analog-to-digital converters," *IEEE Trans. Appl. Supercond.*, vol. 19, pp. 670–675, Jun. 2009.

[40] I. V. Vernik, D. E. Kirichenko, T. V. Filippov, A. Talalaevskii, A. Sahu, A. Inamdar, A. F. Kirichenko, D. Gupta, and O. A. Mukhanov, "Superconducting high-resolution low-pass analog-to-digital converters," *IEEE Trans. Appl. Supercond.*, vol. 17, pp. 442–445, Jun. 2007.

[41] C. Paul, *Fundamentals of Electric Circuit Analysis*. John Wiley and Sons, 2001, pp. 13–17.

[42] P. Longhini, S. Berggren, A. P. A. Leese de Escobar, S. Rice, B. Taylor, V. In, O. A. Mukhanov, G. Prokopenko, M. Nisenoff, E. Wong, and M. de Andrade, "Voltage response of non-uniform arrays of bi-superconductive quantum interference devices," *J. Appl. Phys.*, vol. 111, pp. 093 920 1–14, May 2012.

[43] HYPRES, "Nb process design rules, revision #24," Jan. 11 2008, http://www.hypres.com.

[44] D. Yohannes, S. Sarwana, S. K. Tolpygo, A. Sahu, and V. Semenov, "Characterization of HYPRES' 4.5 kA/cm^2 & 8 kA/cm^2 Nb/AlO$_x$/Nb fabrication processes," *IEEE Trans. Appl. Supercond.*, vol. 15, p. 90, 2005.

[45] D. K. Brock, A. M. Kadin, A. F. Kirichenko, O. A. Mukhanov, S. Sarwana, J. A. Vivalda, W. Chen, and J. E. Lukens, "Retargeting RSFQ cells to a submicron fabrication process," *IEEE Trans. Appl. Supercond.*, vol. 11, no. 1, pp. 369–372, Mar. 2001.

[46] G. V. Prokopenko, O. A. Mukhanov, A. Leese de Escobar, B. Taylor, M. C. de Andrade, S. Berggren, P. Longhini, A. Palacios, M. Nisenoff, and R. L. Fagaly, "DC and RF measurements of serial bi-squid arrays," *IEEE Trans. Appl. Supercond.*, vol. 23, 2013 (in press).

[47] The SQUID Handbook, Vol. II, *Applications of SQUIDs and SQUID Systems*, J. Clarke and A. I. Braginski, Eds. Wiley-VCH, Weinheim, Germany, 2006.

[48] The SQUID Handbook, Vol. I, *Fundamentals and Technology of SQUIDs and SQUID Systems*, J. Clarke and A. I. Braginski, Eds. Wiley-VCH, Weinheim, Germany, 2004.

[49] A. Kamal, J. Clarke, and M. H. Devoret, "Gain, directionality, and noise in microwave SQUID amplifiers: Input-output approach," *Phys. Rev. B*, vol. 86, p. 144510, 2012.

[50] M. Mueck and R. McDermott, "Radio-frequency amplifiers based on DC SQUIDs," *Supercond. Sci. Technol.*, vol. 23, p. 093001, 2010.